ORIGINAL PAPER

The electrochemistry of electrode edges and its relevance to partially blocked voltammetric electrodes

Jan C. Myland · Keith B. Oldham

Abstract Analytical mathematics and digital simulation are used to predict the response, to a potential jump, of the junction between insulating and conducting regions of an electrode. The simulation is carried out differentially and employs other novel features. Concentrations in the vicinity of edges of positive and negative curvatures, as well as straight edges, are analyzed by the model and thereby the faradaic current densities and currents are predicted. It is shown that, in addition to the well-understood cottrellian current arising from the surface of the conducting electrode, currents are generated that are proportional to the length of the edge and to its curvature. These results are then applied to inlaid disks and to partially blocked electrodes. The possibility is explored of using the response to a potential step to gain information on the geometry of a partially blocked electrode.

Keywords Heterogeneous electrodes ·
Partially blocked electrodes · Diffusion · Cottrellian current ·
Digital simulation · Electrode edges · Inlaid disk electrode ·
Prompt current · Potential-jump chronoamperometry

Introduction

Solid electrodes are wont to display heterogeneity for various reasons: on account of the exposure of different crystal faces, from the preferential oxidation of certain sites, from the presence in the conducting phase of impurities or alloying elements, from contamination by detritus, and from other causes. Such surface heterogeneity is, of course, a disquieting complication for electrochemists, though it can sometimes be turned to advantage [1]. The simplest type of inhomogeneity is the partial occlusion of an otherwise uniform electrode by a surface feature that effectively prevents the electrode process from occurring on some fraction of the electrode. This "partial blocking" of an electrode has been examined by a number of authors [2–5] for a variety of repeating or random patterns of the occluding agent. The feature possessed by partially blocked electrodes that is absent from naked electrodes is the pronounced presence of edges; that is, junctions between conducting portions and insulating portions of the surface. The purpose of this article is to examine the electrochemical properties of edges, to show how they affect voltammetry, and to discuss how these properties might illuminate electrode heterogeneity.

Throughout this article, we consider only flat conductors that share their surface with a coplanar insulator. In early sections, attention is confined to a small fragment of edge, but in a later section, we return to the consideration of the electrochemistry of an electrode with multiple edges and show how the chronoamperometric response of a partially blocked electrode can provide information on the configuration of the blockage.

We address edged electrodes, previously inactive, subjected to the simplest voltammetric perturbation—the imposition of a totally concentration-polarizing potential step—but the same principles apply to other experiments. In the immediate aftermath of the potential jump, the faradaic response will be dominated by the cottrellian current arising from the conducting portion of the plane, but as time progresses the current will significantly exceed that predicted by the Cottrell equation. The excess current, beyond the cottrellian component, is associated with the

J. C. Myland · K. B. Oldham (✉)
Department of Chemistry, Trent University,
Peterborough, Ontario, Canada KJ9 7B8
e-mail: koldham@trentu.ca

conductor/insulator junction near which the current density is enhanced. The electrochemistry at such edges has received little voltammetric attention, but is the main preoccupation of the present study.

Figure 1 is a plan view of three edge fragments in which an electronic conductor meets an adjacent insulator. The edge in diagram (ii) is linear, this being the simplest junction between a conductor and a coplanar insulator. In diagram (i), the edge is concave, whereas in (iii) the edge is convex (from the viewpoint of the conductor). A plane edge fragment has two properties: length and curvature. The lengths of the three edges in Fig. 1 are all ℓ. Curvature is assigned to a curve at a particular point by fitting a circle to the curve at the point in question; the magnitude of the curvature is then the reciprocal of the radius of that circle. Sign is (arbitrarily) allocated to the curvature κ such that the edges for cases (i), (ii), and (iii) have positive, zero, and negative curvatures, respectively. An important property of the edge fragment is the product $\kappa\ell$ of its curvature and its length: this is a dimensionless quantity that crops up repeatedly in the present article; it equals the angle through which the edge turns. For the sake of definiteness, we initially choose to study curved edges of a length such that $|\kappa|\ell = 1$, so that the angle turned is one radian, as illustrated. Close to the edge, that is, at small values of x in the three diagrams, the excess current density would be expected to differ minimally from one case compared with another, but as time progresses the three edges will behave differently, in ways that we seek to discover.

There are several elements in the present research. In the first and second sections, the concentration and current density distributions in the vicinity of a straight edge, case (ii), are addressed. This is a topic that can be handled by
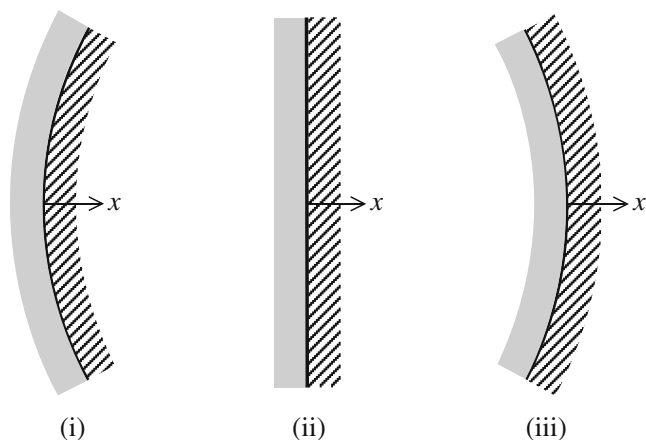

Fig. 1 Each of these three plan diagrams shows a fragment of an edged electrode, each edge being of length ℓ. *Hatching* is used to denote the conductor, whereas the adjoining insulator is shown *shaded*. In (i), the junction is concave with a positive curvature κ; in (ii), the junction is linear ($\kappa=0$); in (iii), the junction is convex with κ negative. In all cases, x represents distance measured normally from the edge across the conducting face of the electrode
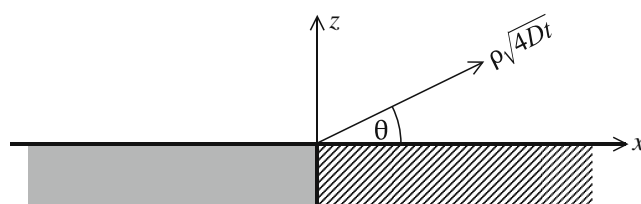
Fig. 2 The cartesian and polar coordinate systems used to analyze straight electrode edges. The y-axis is perpendicular to the plane of the paper. As in Fig. 1, *hatching* represents the conductor with *shading* indicating the insulator. Electrolyte solution occupies the space above the horizontal plane

analytical mathematics. In later sections, we develop and apply "differential simulation" to explore the corresponding properties of curved edges, going on to measure the excess current produced by these edges. Finally, we show how the voltammetric current can throw light on the configuration of a partially blocked electrode.

Concentrations near a straight edge, by mathematical analysis

Because its lack of curvature is a simplifying feature, classical mathematical techniques are able to predict the chronoamperometric response of the edge diagrammed in Fig. 1 (ii). Some 28 years ago, this geometry was investigated [6] but, because that analysis was not entirely convincing, it is treated again here by a superior procedure.

Figure 2 shows a linear edge in three-dimensional cartesian coordinates (x, y, z), with z representing distance from the (insulator or conductor) surface into the electrolyte solution. The $x>0$ half of the $z=0$ plane is occupied by the electrochemically active conducting surface, whereas the $x<0$ half is the surface of a coplanar insulator. Thus, the $(x=0, -\infty<y<\infty, z=0)$ line is the edge separating the two half-planes. An electrolyte solution containing an electrolabile substrate occupies the entire $z\geq0$ space. This solute species had a uniform concentration c^b prior to time $t = 0$; at that instant, the concentration on the electrode surface became zero permanently. Because we are assuming that diffusion is the sole operative transport mechanism, Fick's second law in the form

$$\frac{\partial^2 c}{\partial x^2} + \frac{\partial^2 c}{\partial z^2} = \frac{1}{D}\frac{\partial c}{\partial t} \tag{1}$$

applies, where c denotes the concentration of the electrolabile species and D is its diffusivity. The y coordinate is absent from this equation because translational symmetry exists along that axis. We seek to ascertain the concentration distribution at times $t>0$, especially in the vicinity of the edge.

Because the solution of our problem must be of the form $c=c^b\mathrm{f}(x, z, D, t)$, dimensional constraints make it evident

that the function f must operate on such dimensionless groups as $x/\sqrt{Dt}$, $(z^2+x^2)/(Dt)$ and z/x. By adopting these ratios as the pertinent quantities, the number of independent variables may be reduced to two.

The origin line, $x=z=0$, has no special significance in a cartesian system of coordinates, whereas this line is clearly unique in the chronoamperometric experiment. Accordingly, it is preferable to convert to a polar system, which we do by making the temporary replacements

$$\rho = \sqrt{\frac{x^2 + z^2}{4Dt}} \tag{2}$$

and

$$\theta = \arctan\left(\frac{z}{x}\right) \tag{3}$$

The y coordinate remains an unimportant third dimension. We need to recast Eq. (1) in terms of the new coordinate pair. This task requires straightforward application of standard partial differentiation techniques [7] but, because the derivation is lengthy, details are omitted. The surprisingly simple result is

$$\frac{\partial^2 c}{\partial \rho^2} + \left(\frac{1}{\rho} + 2\rho\right)\frac{\partial c}{\partial \rho} + \frac{1}{\rho^2}\frac{\partial^2 c}{\partial \theta^2} = 0 \tag{4}$$

We seek to solve this equation subject to conditions that apply during our potential-leap experiment. These include the requirement that

$$c = c^b \qquad \rho \to \infty, \quad \theta \neq 0 \tag{5}$$

together with the boundary conditions

$$c = 0 \qquad \theta = 0, \quad \rho \neq 0 \tag{6}$$

and

$$\frac{\partial c}{\partial \theta} = 0 \qquad \theta = \pi, \quad \rho \neq 0 \tag{7}$$

The last two constraints reflect, respectively, the complete concentration polarization of the conductor and the lack of any flux across the insulator surface.

A separability assumption [8, 9] will now be made. By setting

$$c(r,\theta) = c^b \, R(\rho)\Theta(\theta) \tag{8}$$

it is postulated that the bivariate c function can be replaced by a product of two univariate functions. Such an assumption is often, though not always, successful in resolving a partial differential equation into ordinary differential equations. Here, the adoption of (8) leads from (4) to

$$\frac{\rho^2}{R}\frac{d^2 R}{d\rho^2} + \frac{\rho + 2\rho^3}{R}\frac{dR}{d\rho} = \frac{-1}{\Theta}\frac{d^2\Theta}{d\theta^2} \tag{9}$$

The right-hand member of this equation is independent of ρ, whereas its left side is independent of θ. The inescapable conclusion is that each side equals the same constant, which we take to be positive and, for future convenience, represented by $\mu^2/4$.

The equating of the right-hand member of (9) to $\mu^2/4$ leads to

$$\frac{d^2\Theta}{d\theta^2} = \frac{-\mu^2\Theta}{4} \tag{10}$$

Subject to the requirement, stemming from condition (6), that Θ be zero when $\theta=0$, a solution of differential equation (10) is

$$\Theta = (constant)\sin\left\{\frac{\mu\theta}{2}\right\} \tag{11}$$

However, through condition (7), there is also the constraint that $d\Theta/d\theta$ be zero when $\theta=\pi$. This demands that μ be an odd integer of either sign. Inasmuch as negative integers in (11) merely duplicate their positive brethren, we henceforth ignore the negative option and allow μ to adopt solely the values 1, 3, 5,$\cdots$.

When the left-hand moiety of (9) is equated to $\mu^2/4$, that equation becomes

$$\rho^2\frac{d^2 R}{d\rho^2} + \left(\rho + 2\rho^3\right)\frac{dR}{d\rho} - \frac{\mu^2 R}{4} = 0 \qquad \mu = 1, 3, 5, \cdots \tag{12}$$

By making the substitution $R(\rho)=(\rho^2/2)^{\mu/4}H(\rho^2)$ and thereby changing first the dependent and then the independent variable, Eq. (12) is converted first to

$$\rho\frac{d^2 H}{d\rho^2} + \left(1 + \mu + 2\rho^2\right)\frac{dH}{d\rho} + \mu\rho \, H = 0 \tag{13}$$

and thence to

$$\rho^2\frac{d^2 H}{d(\rho^2)^2} + \left(1 + \frac{\mu}{2} + \rho^2\right)\frac{dH}{d(\rho^2)} + \frac{\mu}{4} H = 0 \tag{14}$$

This is a confluent hypergeometric differential equation [10] in $-\rho^2$. Second order ordinary differential equations, such as this, invariably have two alternative solutions, but in this case one of these is imaginary. The real solution is

$$H(\rho^2) = (constant)\exp(-\rho^2) \, M\left(1 + \tfrac{1}{4}\mu, 1 + \tfrac{1}{2}\mu, \rho^2\right) \tag{15}$$

where M(, ,) is a Kummer function [11, chap 47]. Returning to the original radial variable, we find

$$R(\rho) = w_\mu \, \rho^{\mu/2} \exp(-\rho^2) \, M\left(1 + \tfrac{1}{4}\mu, 1 + \tfrac{1}{2}\mu, \rho^2\right) \tag{16}$$

to be the solution to the radial moiety of the straight edge problem. Here w_μ is a presently arbitrary weighting factor

associated with the μ parameter. An alternative representation of R(ρ) makes use of the identity

$$M\left(1+\tfrac{1}{4}\mu, 1 + \tfrac{1}{2}\mu, \rho^2\right) = \Gamma\left(\frac{\mu}{4}+\frac{1}{2}\right)\left[\frac{4}{\rho^2}\right]^{\frac{\mu}{4}-\frac{1}{2}}$$
$$\exp\left(\frac{\rho^2}{2}\right)\left[I_{\frac{\mu}{4}-\frac{1}{2}}\left(\frac{\rho^2}{2}\right) + I_{\frac{\mu}{4}+\frac{1}{2}}\left(\frac{\rho^2}{2}\right)\right] \quad (17)$$

involving a pair of modified Bessel functions [11, chap 50].

We are now in a position to assemble the complete solution. It must be expected that the solution will involve a collection of μ values, rather than just one, so the overall solution is

$$c(r, \theta) = c^b \exp\left(-\rho^2\right)$$
$$\sum_{\mu=1,3,\cdots}^{\infty} w_\mu \, \rho^{\mu/2} M\left(1+\tfrac{1}{4}\mu, 1 + \tfrac{1}{2}\mu, \rho^2\right) \sin\left(\tfrac{1}{2}\mu\theta\right) \quad (18)$$

It remains to identify the w_μ weighting factors, for which purpose condition (5) will be employed. It is known [11, chap 47] that, as its argument u approaches infinity, the Kummer function M(a, c, u) approaches $\Gamma(c)u^{a-c}\exp(u)/\Gamma(a)$ and therefore

$$c(r \to \infty, \theta) = c^b \sum_{\mu=1,3,\cdots}^{\infty} \frac{\Gamma\left(1+\tfrac{1}{2}\mu\right)}{\Gamma\left(1+\tfrac{1}{4}\mu\right)} w_\mu \sin\left(\tfrac{1}{2}\mu\theta\right) \quad (19)$$

where $\Gamma(\ )$ denotes a gamma function [11, chap 43]. To satisfy condition (5), the summation in (19) must equal unity for all non-zero values of θ. On comparison of this equation with the well-known Fourier series

$$\sum_{\mu=1,3,\cdots}^{\infty} \frac{\sin\left(\tfrac{1}{2}\mu\theta\right)}{\mu} = \frac{\pi}{4} \qquad 0 < \theta < \pi \quad (20)$$

it is evident that condition (5) is satisfied only if

$$w_\mu = \frac{4}{\mu\pi}\frac{\Gamma\left(1+\tfrac{1}{4}\mu\right)}{\Gamma\left(1+\tfrac{1}{2}\mu\right)} = \frac{2\Gamma(\mu/4)}{\mu\pi\Gamma(\mu/2)} \qquad \mu = 1, 3, 5, \cdots \quad (21)$$

With this identification inserted, the full solution becomes

$$c(\rho, \theta) = \frac{2c^b}{\pi} \exp\left(-\rho^2\right)$$
$$\sum_{\mu=1,3,\cdots}^{\infty} \frac{\Gamma(\mu/4)}{\mu\Gamma(\mu/2)}\rho^{m/2} M\left(1+\tfrac{1}{4}\mu, 1 + \tfrac{1}{2}\mu, \rho^2\right) \sin\left(\tfrac{1}{2}\mu\theta\right) \quad (22)$$

or, on reverting to the original cartesian coordinates,

$$c(x, z, t) = \frac{2c^b}{\pi} \exp\left\{\frac{-x^2-z^2}{4Dt}\right\} \sum_{\mu=1,3,\cdots}^{\infty} \frac{\Gamma\left(\tfrac{1}{4}\mu\right)}{\mu\Gamma\left(\tfrac{1}{2}\mu\right)}\left(\frac{x^2+z^2}{4Dt}\right)^{\frac{\mu}{4}}$$
$$M\left(1+\frac{\mu}{4}, 1+\frac{\mu}{2}, \frac{x^2+z^2}{4Dt}\right)\sin\left\{\frac{\mu}{2}\text{Arctan}\left(\frac{z}{x}\right)\right\} \quad (23)$$

In comprehensive application, the multivalued Arctan(z/x) function in Eq. (23) is replaced by $\tfrac{1}{2}\pi - \{1+\text{sgn}(x)-\text{sgn}(x^2)\}\{\tfrac{1}{2}\pi - \arcsin(|z|/\sqrt{x^2+z^2})\}$ to permit evaluation for all values of x and z (except when both are zero) and to allow extension to all quadrants of the x, z plane. Although the third or fourth quadrants are of no interest here, it should be noted that Eq. (23) also applies to the problem in which a thin electrode sheet is immersed in an electrolyte solution without any proximal insulator.

As expected, Eq. (23) predicts an approach of $c(x, z, t)$ to c^b at large positive values of z and large negative values of x, whereas in the limit of large positive x, it reduces to the cottrellian result

$$c(x \to \infty, z, t) = c^b \text{erf}\left\{\frac{z}{\sqrt{4Dt}}\right\}$$
$$= \frac{2c^b}{\sqrt{\pi}}\left[\frac{z}{\sqrt{4Dt}} - \frac{1}{3}\left(\frac{z}{\sqrt{4Dt}}\right)^3 + \frac{1}{10}\left(\frac{z}{\sqrt{4Dt}}\right)^5 - \cdots\right] \quad (24)$$

in which erf( ) denotes the error function [11, chap 40]. There is also interest in the concentration profile directly above the edge itself, that is at $x=0$. One finds from Eq. (23) that

$$c(0, z, t) = \frac{\sqrt{2}c^b}{\pi} \exp\left\{\frac{-z^2}{4Dt}\right\}$$
$$\sum_{\mu=1,3,\cdots}^{\infty} (-)^{\text{Int}\{(\mu-1)/4\}} \frac{\Gamma(\mu/4)}{\mu\Gamma(\mu/2)}\left(\frac{z^2}{4Dt}\right)^{\frac{\mu}{4}}$$
$$M\left(1+\frac{\mu}{4}, 1+\frac{\mu}{2}, \frac{z^2}{4Dt}\right)$$
$$= \frac{\sqrt{2}c^b}{\pi^{3/2}}\left[\Gamma(\tfrac{1}{4})\left(\frac{z}{\sqrt{4Dt}}\right)^{1/2} + \frac{2\Gamma(\tfrac{3}{4})}{3}\left(\frac{z}{\sqrt{4Dt}}\right)^{3/2}\right.$$
$$\left. - \frac{\Gamma(\tfrac{1}{4})}{10}\left(\frac{z}{\sqrt{4Dt}}\right)^{5/2} - \cdots\right] \quad (25)$$

A diagram illustrating Eq. (25) appears later in this article. Note an important distinction between the last two equations. Whereas in (24), remote from the edge, the concentration profile obeys a polynomial expansion in odd powers of $z/\sqrt{4Dt}$, the powers involved *at* the edge are *half*-odd powers. One consequence of this is that the concentration gradient (and thence the current density) is infinite at the edge.

Figure 3 is a three-dimensional plot of Eq. (23). It suggests that the infinite concentration gradient is restricted to the $(x, z)=(0, 0)$ line, and this is confirmed by the expansions

$$\frac{c(x, z, t)}{c^b} = \sqrt{\frac{X}{\pi^3}}\left[\{\Gamma(\tfrac{1}{4}) + 2\Gamma(\tfrac{3}{4})X + O(X^2)\}\frac{z}{x}\right.$$
$$\left. - \left\{\frac{\Gamma(\tfrac{1}{4})}{8} - \frac{\Gamma(\tfrac{3}{4})X}{12} + O(X^2)\right\}\frac{z^3}{x^3} + O\left(\frac{z^5}{x^5}\right)\right] \quad (26)$$
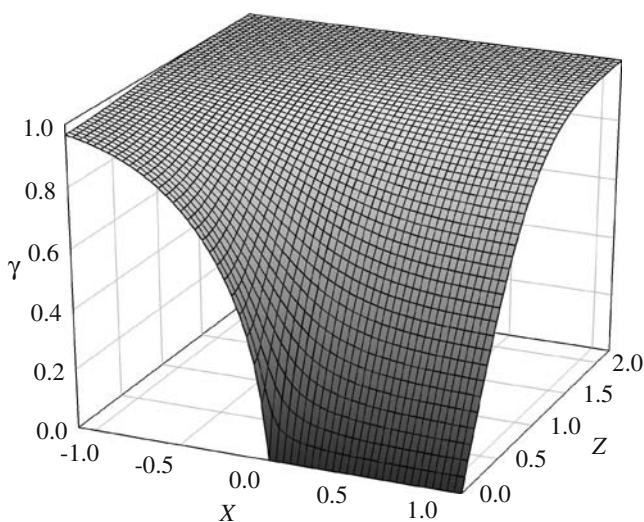
Fig. 3 A three-dimensional plot showing the distribution of concentration close to a totally concentration-polarized straight edge. Insulator occupies the half-plane $z=0$, $x<0$, the conducting portion of the electrode being $z=0$, $x>0$. The axes, labeled X, Z, and γ, are $x/\sqrt{4Dt}$, $z/\sqrt{4Dt}$, and c/c^b

and

$$\frac{c(x,z,t)}{c^b} = \sqrt{\frac{-X}{\pi^3}} \left[\begin{array}{l} 2\Gamma\left(\frac{1}{4}\right) - \frac{4\Gamma\left(\frac{3}{4}\right)X}{3} + O(X^2) \\ + \left\{ \frac{\Gamma\left(\frac{1}{4}\right)}{4} - \frac{\Gamma\left(\frac{3}{4}\right)X}{2} + O(X^2) \right\} \frac{z^2}{x^2} \\ - \left\{ \frac{5\Gamma\left(\frac{1}{4}\right)}{64} + \frac{\Gamma\left(\frac{3}{4}\right)X}{32} + O(X^2) \right\} \frac{z^4}{x^4} + O\left(\frac{z^6}{x^6}\right) \end{array} \right]$$

(27)

describing the concentration profiles close to the edge on the conductor and insulator sides, respectively. In these equations, and elsewhere, X is used to abbreviate $x/\sqrt{4Dt}$, x being negative in (27). Notice that, as might have been expected, only odd powers of z appear in (26), whereas only even powers (including zero) are found in (25). It is amazing that, as x approaches zero from either direction, each of Eqs. (26) and (27) passes smoothly into (25).

Embodied in Eq. (23) is the requirement that there is no flux of the electrolabile species across the insulating, $x<0$, portion of the electrode surface, whereas there is such a flux across the conducting, as $x>0$, portion. The latter flux is proportional to the current density, as we show in the next section.

Excess current from the straight edge, by mathematical analysis

In this section, analytical techniques will be used to evaluate the current density, and thence the current, flowing to the straight-edged electrode. This evaluation will be based on the analytical results from the previous section,

but subsequently we will derive similar results by digital simulation. The current will be shown to contain a cottrellian portion and a "prompt" component, proportional to the length of the edge.

Differentiation with respect to z of Eq. (23) yields

$$\frac{\partial c}{\partial z}(x>0, z=0, t) = \frac{c^b}{\pi x} \exp\left(\frac{-x^2}{4Dt}\right)$$
$$\sum_{\mu=1,3,\cdots}^{\infty} \frac{\Gamma\left(\frac{1}{2}\mu\right)}{\Gamma\left(\frac{1}{2}\mu\right)} \left(\frac{x^2}{4Dt}\right)^{\mu/4} M\left(1+\frac{\mu}{4}, 1+\frac{\mu}{2}, \frac{x^2}{4Dt}\right)$$

(28)

after z is set to zero. A second representation of this result is

$$\frac{\partial c}{\partial z}(x>0, z=0, t) = \frac{c^b}{\sqrt{4\pi Dt}} \exp\left(\frac{-x^2}{8Dt}\right)$$
$$\sum_{\mu=1,3,\cdots}^{\infty} I_{\frac{\mu}{4}-\frac{1}{2}}\left(\frac{x^2}{8Dt}\right) + I_{\frac{\mu}{4}+\frac{1}{2}}\left(\frac{x^2}{8Dt}\right)$$

(29)

a third, incorporating an integral that involves the Macdonald function [11, chap 51] of one-quarter order, is

$$\frac{\partial c}{\partial z}(x>0, z=0, t)$$
$$= \frac{c^b}{\sqrt{\pi Dt}} \left[1 + \frac{1}{\sqrt{32\pi}} \int_{x^2/8Dt}^{\infty} \frac{\exp(-\lambda)}{\lambda} K_{1/4}(\lambda) d\lambda \right]$$

(30)

while a fourth, in which the $X = x/\sqrt{4Dt}$ abbreviation is reused,

$$\frac{\partial c}{\partial z}(x>0, z=0, t) = \frac{c^b}{\sqrt{4\pi Dt}} \left[\begin{array}{l} \frac{\sqrt{2/X}}{\Gamma\left(\frac{3}{4}\right)} \sum_{j=0}^{\infty} \frac{\left(\frac{-1}{4}\right)_j \left(\frac{1}{4}\right)_j (-X^2)^j}{\left(\frac{1}{2}\right)_j \left(\frac{3}{4}\right)_j (1)_j} \\ + \frac{\sqrt{X/2}}{\Gamma\left(\frac{5}{4}\right)} \sum_{j=0}^{\infty} \frac{\left(\frac{1}{4}\right)_j \left(\frac{3}{4}\right)_j (-X^2)^j}{(1)_j \left(\frac{5}{4}\right)_j \left(\frac{3}{2}\right)_j} \end{array} \right]$$

(31)

incorporates a pair of hypergeometric functions [11, chap 18]. Surprisingly, this disparate quartet of representations can be confirmed to be identical numerically. All four expressions approach the cottrellian formula $c^b/\sqrt{\pi Dt}$ at large x and, in accord with Eq. (25), become infinite at $x=0$.

Formula (30) is especially suitable for expressing the difference between the concentration gradient and that for the cottrellian case. One thereby finds that

$$\frac{\partial c}{\partial z}(x>0, z=0, t) - \frac{\partial c}{\partial z}_{\text{cot}}(z=0, t)$$
$$= \frac{c^b}{\sqrt{32\pi^3 Dt}} \int_{x^2/8Dt}^{\infty} \frac{\exp(-\lambda)}{\lambda} K_{1/4}(\lambda) d\lambda$$

(32)

represents the additional current density due to the proximity of the straight edge.

If the electrode reaction involves a single electron, then by Fick's first and Faraday's laws, the current density $i(x, t)$ may be found by multiplying the concentration gradient at the conductor surface by the diffusivity D and Faraday's constant F:

$$i(x, t) = FD \frac{\partial c}{\partial z}(x, 0, t) \qquad (33)$$

Figure 4 plots the ratio of this current density to the cottrellian current density, the latter being

$$i_{cot}(t) = Fc^b \sqrt{\frac{D}{\pi t}} \qquad (34)$$

[12] and shows how the ratio varies with distance from the edge. Notice that the current density departs significantly from its cottrellian value only over a strip of about $3\sqrt{Dt}$ width. Recognize that, although the current density *at* the edge is infinite, this is still a trivial contribution to the current enhancement. Notwithstanding the title given to this section, the excess current arises from the narrow strip fringing the edge, not "from" the edge itself.

Multiplying equation (32) by FD leads to the formula

$$
\begin{aligned}
i(x, t) - i_{cot}(t) &= Fc^b \sqrt{\frac{D}{32\pi^3 t}} \int_{x^2/8Dt}^{\infty} \frac{\exp(-\lambda)}{\lambda} K_{1/4}(\lambda) d\lambda \\
&= \frac{i_{cot}(t)}{\sqrt{32\pi}} \int_{x^2/8Dt}^{\infty} \frac{\exp(-\lambda)}{\lambda} K_{1/4}(\lambda) d\lambda
\end{aligned}
$$

$$(35)$$

Our prime interest is in the magnitude of the excess current, over and above the cottrellian contribution, arising from this
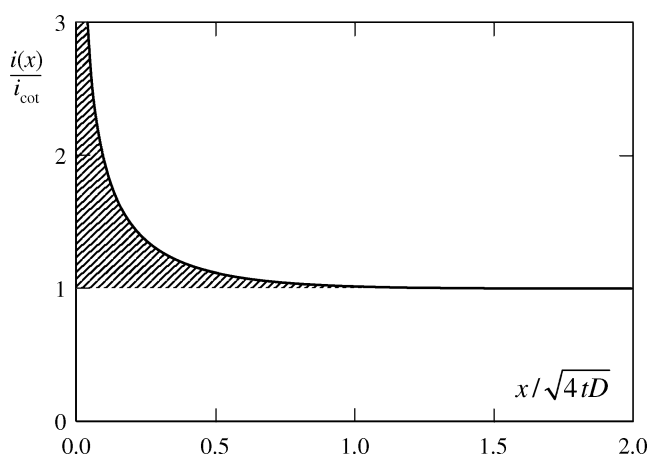

Fig. 4 The current density close to a straight edge normalized by division by the cottrellian current i_{cot}. The *shaded area* corresponds to the "excess current" $\hat{I}(t, ii)$ ascribable to the edge

current density. To find this excess current, to which we give the symbol $\hat{I}(t)$, one first needs to integrate the expression in (35) between the limits of $x=0$ and $x=\infty$, as the shading in Fig. 4 suggests. The result is remarkably simple

$$
\begin{aligned}
\int_0^{\infty} [i(x, t) - i_{cot}(t)] dx &= Fc^b \sqrt{\frac{D}{32\pi^3 t}} \int_0^{\infty} \int_{x^2/8Dt}^{\infty} \frac{\exp(-\lambda)}{\lambda} K_{1/4}(\lambda) d\lambda dx \\
&= \frac{Fc^b D}{2}
\end{aligned}
$$

$$(36)$$

This result has been obtained before [6] while Gavaghan and Rollett [17] approached the problem differently. The quantity in Eq. (36) is a lineal current density, with the ampere per meter unit. To obtain the excess current $\hat{I}(t)$ itself, this lineal current density must be multiplied by the length ℓ of the edge fragment, corresponding to the chosen interval in the y direction. This choice leads to a current

$$\hat{I}(t) = \frac{Fc^b D\ell}{2} \qquad (37)$$

Note the time independence of this excess current. It appears at the instant $t=0$ and continues constantly thereafter, earning it the title "prompt current" [12]. It should be appreciated that this is an exact result. The current from a straight-edged electrode consists solely of the cottrellian current plus the prompt current given by (37); these are not just the first two terms in an expansion. However, it is to be expected that curvature in an edge will introduce one or more additional time-dependent terms. The search for these terms starts with the next section.

Concentrations near edges of any curvature, by simulation

Our focus now shifts to the edges diagrammed as (i) and (iii) in Fig. 1, though the simulation described below also serves case (ii), the straight edge. A comparison of our modelling results detailed here, with the analysis carried out in earlier sections, will validate the simulation procedure.

Previously in this study, cartesian and polar coordinates have been employed but now we turn to cylindrical coordinates, in which Fick's second law is

$$
\begin{aligned}
\frac{1}{D} \frac{\partial c}{\partial t}(r, z, t) &= \nabla^2 c(r, z, t) \\
&= \frac{\partial^2 c}{\partial r^2}(r, z, t) + \frac{1}{r} \frac{\partial c}{\partial r}(r, z, t) + \frac{\partial^2 c}{\partial z^2}(r, z, t)
\end{aligned}
$$

$$(38)$$

This is the most appropriate coordinate system for treating the curved edges shown in diagrams (i) and (iii) of Fig. 1. In application to curved edges, r represents distance

measured from the edge's centre of curvature. We can adapt Eq. (38) better to suit our purpose by replacing r by $x - (1/\kappa)$ for case (i) and case (iii), x being the distance coordinate identified in Fig. 1. With this definition, differential equation (38) becomes

$$\frac{1}{D}\frac{\partial c}{\partial t}(x,z,t) = \frac{\partial^2 c}{\partial x^2}(x,z,t) - \frac{\kappa}{1-\kappa x}\frac{\partial c}{\partial x}(x,z,t) + \frac{\partial^2 c}{\partial z^2}(x,z,t)$$
(39)

this equation being applicable not only to both curved cases, but also to case (ii). The inclusion of the straight edge case arises because, when $\kappa=0$, the term in this equation representing the cylindricity of the system disappears, leaving the cartesian version of Fick's second law. Thus, Eq. (39) applies to all three of the geometries in Fig. 1. In this equation, $x=0$ corresponds to the edge, $x<0$ to the domain over the insulator, and $x>0$ to the domain over the conductor.

Because a representation in cylindrical coordinates is then no longer appropriate, Eq. (39) ceases to make sense where $x>1/\kappa$ for case (i), or where $x<1/\kappa$ for case (iii). This is not a limitation in the present study, however, because our interest is confined to the narrow fringes of insulator and conductor on either side of the edge.

The initial condition,

$$c(x,z,t) = c^{\mathrm{b}}, \quad 0 < z \le \infty, \quad \text{all } x, \quad t \le 0$$
(40)

prescribing a preexisting concentration uniformity, applies. The crucial boundary conditions are

$$c(x,0,t) = 0 \quad x > 0, \quad t > 0$$
(41)

and

$$\frac{\partial c}{\partial z}(x,0,t) = 0 \quad x < 0, \quad t > 0$$
(42)

which respectively assert that the electrolabile species is absent from the electrode surface and has no flux across the insulator surface.

An analytical solution may exist to the equation set (39)–(42) but, at this juncture, we have found it only for the $\kappa=0$ instance, as reported above. Therefore, we turn to digital simulation and seek an approximate prediction. As in most simulations [14], the first and second steps are to undimension and then discretize the variables. The three independent variables and the one dependent variable are undimensioned through the definitions

$$\tau = \frac{Dt}{\ell^2}, \quad \zeta = \frac{z}{\ell}, \quad \chi = \frac{x}{\ell} \quad \text{and} \quad \gamma(\chi,\zeta,\tau) = \frac{c(x,z,t)}{c^{\mathrm{b}}}$$
(43)

Note that χ cannot exceed $1/\kappa\ell$ in case (i) and must exceed $-1/\kappa\ell$ in case (iii), there being no restriction in case (ii). These constraints arise because it is implicit in Eq. (39) that

r be non-negative. For the sake of uniformity, the condition $(-1/|\kappa|\ell) < \chi < (1/|\kappa|\ell)$ is applied universally in this section and, in view of the standard length ℓ that we adopt, this implies that our simulation domain occupies the region

$$-1 < \chi < 1$$
(44)

Adoption of the dimensionless terms defined in (43) converts the differential equation (39) into

$$\frac{\partial^2\gamma}{\partial\chi^2}(\chi,\zeta,\tau) - \frac{\kappa\ell}{1-\kappa\ell\chi}\frac{\partial\gamma}{\partial\chi}(\chi,\zeta,\tau) + \frac{\partial^2\gamma}{\partial\zeta^2}(\chi,\zeta,\tau)$$
$$- \frac{\partial\gamma}{\partial\tau}(\chi,\zeta,\tau) = 0$$
(45)

while its attendant conditions, stemming from formulas (39–42) become

$$\gamma(\chi,\zeta,0) = 1 \quad -1 < \chi < 1, \quad \zeta > 0$$
(46)

$$\gamma(\chi,0,\tau) = 0 \quad 0 < \chi < 1, \quad \tau > 0$$
(47)

and

$$\frac{\partial\gamma}{\partial\zeta}(\chi,0,\tau) = 0 \quad -1 < \chi < 0, \quad \tau > 0$$
(48)

It is this set of equations that is modelled for each of the three cases, with $\kappa\ell$ set to 1, 0, or −1 for cases (i), (ii), and (iii), respectively.

Discretization of the four dimensionless variables is accomplished by the replacements

$$\tau \Rightarrow k\delta, \quad \zeta \Rightarrow m\Delta, \quad \chi \Rightarrow n\Delta, \quad \text{and} \quad \gamma(\chi,\zeta,\tau) \Rightarrow \gamma_{n,m,k}$$
(49)

in which variables that actually change continuously are substituted by quantities whose values change stepwise. Here $k = 1,3,5,\cdots$, $m = 1,3,5,\cdots$, and $n = \cdots -5,-3,-1,+1,+3,+5,\cdots$. Note our addiction to odd indices. The dimensionless δ and Δ quantities are small time and distance units respectively, of arbitrary magnitude. We choose Δ to be the reciprocal of a large even integer, typically 1,000 and, for a reason discussed later, we set $\delta= 2\Delta^2/5$.

For simplicity, and in line with a philosophy enunciated earlier [15], we employ the oldest, slowest, and most elementary modelling technique: fully explicit finite-difference digital simulation. We toyed with non-uniform grids, but discarded that computation-time-saving strategy in view of the added complication. There are only three non-standard features of our simulation. Our simulation is "differential", rather than absolute. The boundaries of our active simulation space adapt to need. And our procedure for fitting the concentration normal to the conductor surface

is to an unusual "013 polynomial". These three abnormal features are elaborated below. The simulation was programmed straightforwardly in Visual Basic® and executed on a standard PC.

In addition to the two-dimensional array dedicated to the modelling of the set of equations numbered (44) through (47), we also employed a one-dimensional array whereby we simulated the equation set

$$\frac{\partial^2 \beta}{\partial \zeta^2}(\zeta, \tau) - \frac{\partial \beta}{\partial \tau}(\zeta, \tau) = 0 \tag{50}$$

$$\beta(\zeta, \tau) = 1 \quad 0 < \zeta < \infty, \quad \tau = 0 \tag{51}$$

and

$$\beta(\zeta, \tau) = 0 \quad \zeta = 0, \quad \tau > 0 \tag{52}$$

thereby modelling the Cottrell experiment. Here β signifies the undimensioned cottrellian concentration $(c/c^b)_{\text{cot}}$, discretized as $\beta_{m,k}$. The Cottrell simulation is run consecutively with the two-dimensional simulation because interest is in the *difference* between the two current densities. Moreover, a comparison is continually made between corresponding concentrations in the β and γ arrays as a means of economizing computation time, as described below.

In the nomenclature of Britz [14], our simulation employs the "point" method, rather than the "box" method, though it does benefit from some of the advantages of the latter by positioning the first sampling points in both the χ and ζ directions at the half-standard distances of Δ. The grid used in the simulation is shown in Fig. 5. In principle, the simulation domain could extend limitlessly in the ζ (upwards) direction and at least as far as $n = \pm 1/(|\kappa|\ell\Delta)$ in the $\pm\chi$ (sideways) directions, but in practice only a much smaller rectangular subset is employed in early simulation

cycles. The *even* integers L, M, and N (L is negative), which delineate the boundaries of the simulation domain $L < n < N$, $0 < m < M$, are updated (incremented by 2 for M and N, but by −2 for L), if necessary, after each sequence of concentration calculations, to meet the requirement that no value of $\gamma_{L-1,m,k}$ or $\beta_{M+1,k}$ may differ from unity by more than 0.01%, while $\gamma_{N+1m,k}$ may not differ from $\beta_{m,k}$ by a similar percentage.

To discretize the first two terms in differential equation (45), we follow a procedure that leads to results commonly encountered in electrochemical simulations, though they are generally derived differently. The quadratic function $\gamma = a_0 + a_1(\chi/\Delta) + a_2(\chi/\Delta)^2$ is fitted to the trio of concentration values $\gamma_{n+2,m,k}$, $\gamma_{n,m,k}$ and $\gamma_{n-2,m,k}$. The resulting function, namely

$$\gamma \approx a_0 + \frac{(1-n)\gamma_{n+2,m,k} - (1+n)\gamma_{n-2,m,k} + 2n\gamma_{n,m,k}}{4\Delta}\chi$$
$$+ \frac{\gamma_{m,n+2,k} + \gamma_{m,n-2,k} - 2\gamma_{m,n,k}}{8\Delta^2}\chi^2 \tag{53}$$

(a_0 is also calculable, but is unimportant) then serves to model the horizontal distribution of the concentration. On the assumption that this quadratic approximation applies adequately in the vicinity of the (n, m, k) point, the discretization

$$\left(\frac{\partial^2 \gamma}{\partial \chi^2} - \frac{\kappa\ell}{1-\kappa\ell\chi}\frac{\partial \gamma}{\partial \chi}\right)_{n,m,k}$$
$$\Rightarrow \frac{1}{4\Delta^2}\left[\begin{array}{c}\left(1 - \frac{\kappa\ell\Delta}{1-n\kappa\ell\Delta}\right)\gamma_{n+2,m,k} - 2\gamma_{n,m,k} \\ + \left(1 + \frac{\kappa\ell\Delta}{1-n\kappa\ell\Delta}\right)\gamma_{n-2,m,k}\end{array}\right] \tag{54}$$

follows. Note that, because of our chosen $|\kappa|\ell = 1$ standard, the quantity $\kappa\ell$ in (54) and elsewhere always takes one of the three values 1, 0, or −1 depending on the case in question. Generally, a fit of three points to a quadratic

Fig. 5 A small portion of the grid used in the edge simulation. The column indexed "$n=\infty$" is employed for modelling β, the cottrellian concentrations. The outer and upper simulation bounds of the ranges $L < n < N$ and $0 < m < M$ are shown in their initial locations, but these are continually updated as the simulation proceeds
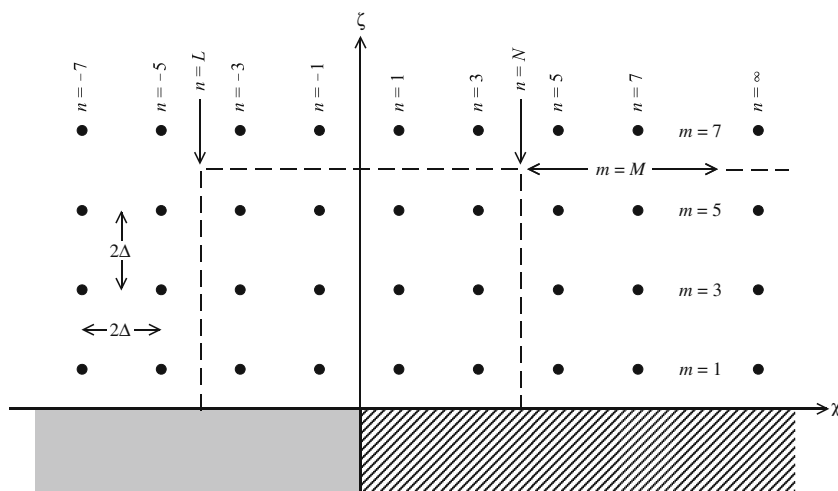
function also provides the basis for discretizing the third term in differential equation (45). This leads to the familiar result

$$\left(\frac{\partial^2 \gamma}{\partial \zeta^2}\right)_{n,m,k} \quad \Rightarrow \quad \frac{\gamma_{n,m+2,k} - 2\gamma_{n,m,k} + \gamma_{n,m-2,k}}{4\Delta^2} \quad (55)$$

To discretize the final right-hand term in Eq. (45), the temporal derivative is replaced by a simple forward difference quotient:

$$\frac{\partial \gamma}{\partial \tau}(\zeta, \chi, \tau) \quad \Rightarrow \quad \frac{\gamma_{n,m,k+2} - \gamma_{n,m,k}}{2\delta} \quad (56)$$

This completes the tally of terms in Eq. (45) for which we have derived discretized equivalents. Putting them all together leads, after rearrangement, to

$$\gamma_{n,m,k+2} = \gamma_{n,m,k} + \frac{\delta}{2\Delta^2}\left[\begin{matrix} c_1\gamma_{n+2,m,k} + c_2\gamma_{n-2.m.k} + c_3\gamma_{n,m+2,k} \\ + c_4\gamma_{n,m-2,k} - c_5\gamma_{n,m,k} \end{matrix}\right] \quad (57)$$

with the coefficients $c_{1,2,-,5}$ given the values listed in the first row of Table 1. Equation (57) shows how, during an interval of duration 2δ, each typical point interacts diffusionally with its four neighboring points (in reality each "point" is a fragment of a circular hoop, except for the straight-edge case, in which it is a straight line fragment). The formula must be modified when $m=1$, because such points have only three neighbors. There are two revised formulas, depending on whether the $m=1$ point is adjacent to the insulator or the conductor. These revisions are discussed in the next paragraph and the resulting coefficients are presented as the second and third rows of Table 1. The final two rows in the table provide coefficients for the corresponding terms in the β-updating formulas.

Points for $m=1$ have only three neighbors because of the proximity of the insulator or the conductor. For the points adjacent to the insulator, the replacement formula, incorporated into the second row of Table 1, was constructed straightforwardly by discretizing the $\partial^2 \gamma/\partial \zeta^2$ term and assigning a concentration gradient of zero to a fitted quadratic at $\zeta=0$. For those $m=1$ points adjacent to the conductor, we discretized the $\partial^2 \gamma/\partial \zeta^2$ portion of Eq. (45)—

and also the $\partial^2 \beta/\partial \zeta^2$ term in (50)—by abandoning quadratic fitting in favor of a fit to the

$$\gamma = b_0 + b_1\frac{\zeta}{\Delta} + b_3\left(\frac{\zeta}{\Delta}\right)^3 \quad (58)$$

polynomial. Our preference for this "013 polynomial" derives from the match that it provides to the second and third terms in Eq. (26). To obtain a good match to reality in the region adjoining the conductor is crucial, because this is the region from which the faradaic current arises. The b coefficients can be evaluated by fitting to the $m=1$ and $m=3$ points and constraining the polynomial to pass through zero at $\zeta=0$. With 013 polynomial fitting, this leads to the simulation formula

$$\left(\frac{\partial^2 \gamma}{\partial \zeta^2}\right)_{n,1,k} \quad \Rightarrow \quad \frac{\gamma_{n,3,k} - 3\gamma_{n,1,k}}{4\Delta^2} \quad (59)$$

Had we used the customary quadratic (or "012 polynomial") fit, the "4" in (59) would have been replaced by a "3". This provides the basis for the third row of entries in Table 1. It may seem irrational to use a 013 polynomial to fit the vertical concentration profile in the vicinity of the $m=1$ point, but revert to the quadratic fit for $m=3, 5, -$. Surprisingly, however, both the 012 and 013 polynomials lead to identical formulas, namely Eq. (55), at points other than those adjacent to the electrode.

There is danger of instability in a simulation if the coefficient of any concentration term in the concentration-updating equations is negative. In our particular problem, this implies that $1 - (c_5\delta/2\Delta^2) \geq 0$. This consideration dictated our choice of $\delta = 2\Delta^2/5$ as the relationship between the magnitudes of the dimensionless time and distance units.

To validate our simulation, we compared concentrations calculated exactly from the mathematical theory with those generated by simulation for the straight edge, case (ii). Because it is the most crucial location for the simulation, and this is where the largest discretization errors might be expected, we chose to compare *at* the edge itself, where $x=\chi=0$. Figure 6 makes the comparison. The line in this figure is calculated from the full Eq.

Table 1 Coefficients of the five terms in Eq. (57) during the simulation of the points indexed n and m

n	m	c_1	c_2	c_3	c_4	c_5
$L+1, \cdots, -3, -1, 1, 3, \cdots, N-1$	$3, 5, \cdots, M-1$	$1 - \frac{\kappa\ell\Delta}{1-n\kappa\ell\Delta}$	$1 + \frac{\kappa\ell\Delta}{1-n\kappa\ell\Delta}$	1	1	4
$-1, -3, \cdots, L+1$	1	$1 - \frac{\kappa\ell\Delta}{1-n\kappa\ell\Delta}$	$1 + \frac{\kappa\ell\Delta}{1-n\kappa\ell\Delta}$	1	No such point	3
$1, 3, \cdots, N-1$	1	$1 - \frac{\kappa\ell\Delta}{1-n\kappa\ell\Delta}$	$1 + \frac{\kappa\ell\Delta}{1-n\kappa\ell\Delta}$	1	No such point	5
∞	$3, 5, \cdots, M-1$	No such point	No such point	1	1	2
∞	1	No such point	No such point	1	No such point	3

The final two rows relate to the one-dimensional simulation of concentration β
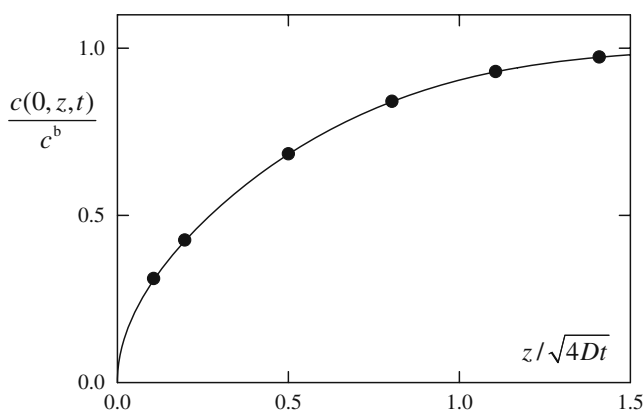
Fig. 6 A simulation/theory comparison of the concentration profile above the straight-edge junction between the conducting portion of an electrode and its adjoining coplanar insulator. The *full curve* is by Eq. (25), *points* are based on the simulation

(25). Because our simulation uses no points at $\chi=0$, the dots represent the average of the simulated concentrations for points indexed $n=-1$ and $n=+1$. There are small discrepancies between theory and simulation, particularly at small ζ, but the general agreement gave us the confidence to proceed.

Concentration gradients at the conductor surface follow directly from differentiating the fitted 013 polynomials and then substituting $\zeta=0$. As our interest is in the difference between the edged cases and the unedged (cottrellian) case, it is the difference, namely

$$\left(\frac{\partial\gamma}{\partial\zeta}\right)_{n,0,k} - \left(\frac{\partial\beta}{\partial\zeta}\right)_{0,k} \Rightarrow \frac{27(\gamma_{n,1,k}-\beta_{1,k})-\gamma_{n,3,k}+\beta_{3,k}}{24\Delta} \tag{60}$$

in the concentration gradients that is calculated. The influence of using the 013 polynomial is pronounced here. Had we employed a quadratic fit, the "27" and "24" in expression (60) would have been "9" and "6".

To reestablish contact with reality, let us clarify exactly what (60) means. The right-hand side of this expression is a model intended to supply approximate values of the difference between the undimensioned concentration gradient on the conductor surface at a finite distance x from the edge and the corresponding (cottrellian) value remote from the edge. Slightly different values result from the three different cases and they arise by ascribing different values (1 or 0 or -1) to $\kappa\ell$. All three cases are simulated in our study. Translating to physical variables

$$\frac{\ell}{c^{\mathrm{b}}}\left[\frac{\partial c}{\partial z}(x,z=0,t) - \frac{\partial c}{\partial z}_{\mathrm{cot}}(z=0,t)\right]$$
$$\Rightarrow \frac{27(\gamma_{n,1,k}-\beta_{1,k})-\gamma_{n,3,k}+\beta_{3,k}}{24\Delta} \tag{61}$$

It is the quantities $\left[27(\gamma_{n,1,k}-\beta_{1,k})-\gamma_{n,3,k}+\beta_{3,k}\right]/(24\Delta)$ that, for all positive odd n less than N and each selected k, are the outputs of the simulation, but they are not saved as such. Instead, each value of (61) becomes a component of the weighted sum

$$2\Delta \sum_{n=1,3,\cdots}^{N-1} W_{n,k} \frac{27(\gamma_{n,1,k}-\beta_{1,k})-\gamma_{n,3,k}+\beta_{3,k}}{24\Delta} \tag{62}$$

For most values of n, the weights $W_{n,k}$ are given by the very elaborate formula

$$W_n = \frac{\sqrt{n}[1-(n-1)\kappa\ell\Delta]}{\sqrt{n}-\sqrt{n-2}} - \sqrt{n^2-2n}\left[1-\frac{2n-2+\sqrt{n^2-2n}}{3}\kappa\ell\Delta\right]$$
$$- \frac{\sqrt{n}[1-(n+1)\kappa\ell\Delta]}{\sqrt{n+2}-\sqrt{n}}$$
$$+ \sqrt{n^2+2n}\left[1-\frac{2n+2+\sqrt{n^2+2n}}{3}\kappa\ell\Delta\right]$$
$$n=5,7,9,\cdots,N-3 \tag{63}$$

the origin of which is explained in the next section. The sources of the abnormal weights, which are

$$W_1 = \frac{3}{\sqrt{3}-1}\left[\frac{1}{2}-\frac{\kappa\ell\Delta}{4}\right] \tag{64}$$

$$W_3 = \frac{3}{\sqrt{3}-1}\left[\frac{\sqrt{3}}{2}-1-\frac{\sqrt{27}-4}{4}\kappa\ell\Delta\right]$$
$$- \frac{\sqrt{3}[1-4\kappa\ell\Delta]}{\sqrt{5}-\sqrt{3}} + \sqrt{15}\left[1-\frac{8+\sqrt{15}}{3}\kappa\ell\Delta\right] \tag{65}$$

and

$$W_{N-1} = \frac{\sqrt{N-1}[1-(N-1)\kappa\ell\Delta]}{\sqrt{N-1}-\sqrt{N-3}}$$
$$- \sqrt{N^2-4N+3}$$
$$\times \left[1-\frac{2N-4+\sqrt{N^2-4N+3}}{3}\kappa\ell\Delta\right] \tag{66}$$

are also explained below. The purpose of the weighting is to prepare the concentration-gradient differences for subsequent conversion to a current, as described in the next section. Only the sums of the weighted quantities are retained by the program.

Excess current from curved edges, via simulated concentrations

Our attention in this section is directed first to the excess current density, beyond that for the cottrellian case,

flowing across the conductor surface at a distance x from the edge and at a time t after the potential jump. We shall represent this current density difference by the "hatted" symbol

$$\hat{\imath}(x,t) = i(x,t) - i_{\text{cot}}(t) = i(x,t) - Fc^{\text{b}}\sqrt{D/\pi t} \qquad (67)$$

Though the cottrellian current density is known analytically, it is the simulated version that is subtracted, the better to compensate for discretization errors. Mostly, we work with a dimensionless current density difference, undimensioned by division by $Fc^{\text{b}}D/\ell$ and represented by a hatted iota symbol. Because we are treating a one-electron reaction, multiplication by FD is all that is required to convert an electrode-surface concentration gradient into a current density; thus:

$$\hat{\imath}(\chi,\tau) = \frac{\ell\,\hat{\imath}(x,t)}{Fc^{\text{b}}D} = \frac{\ell}{c^{\text{b}}}\left[\frac{\partial c}{\partial z}(x,z=0,t) - \frac{\partial c}{\partial z_{\text{cot}}}(z=0,t)\right] \quad (68)$$

Each of our simulations generates a set of values of $\hat{\imath}(\chi,\tau)$ at χ values of $\Delta, 3\Delta, 5\Delta, \cdots, n\Delta, \cdots$ and at a set of τ values equal to $k\delta$ for odd integers k. Members of this discrete set of discretized undimensioned current density differences are symbolized $\hat{\imath}_{n,k}$. Thus, from Eqs. (67) and (61),

$$\hat{\imath}_{n,k} = \frac{27(\gamma_{n,1,k} - \beta_{1,k}) - \gamma_{n,3,k} + \beta_{3,k}}{24\Delta} \qquad (69)$$

Prior to weighting, the output of the simulation is simply the undimensioned current density difference, and so a set of values of $\hat{\imath}(\phi,\tau)$ at χ values of $\Delta, 3\Delta, 5\Delta, \cdots, n\Delta, \cdots$ is accessible for a set of τ values equal to $k\delta$ for odd integers k.

Areal integration is required to convert the excess current density into the excess current $\hat{I}(t)$ associated with the edges. We make this conversion for the three cases, symbolizing the results by $\hat{I}(t,\text{i})$, $\hat{I}(t,\text{ii})$ and $\hat{I}(t,\text{iii})$. The formula

$$\hat{I}(t) = \ell \int_{0}^{3\sqrt{Dt}} \hat{\imath}(x,t)[1 - \kappa x]\,\mathrm{d}x = Fc^{\text{b}}D\ell \int_{0}^{3\sqrt{\tau}} \hat{\imath}(\chi,\tau)[1 - \kappa\ell\chi]\,\mathrm{d}\chi \qquad (70)$$

applies, with the term $[1-\kappa x]$ allowing for the convergent (case i), uniform (case ii), or divergent (case iii) integration domain. The upper integration bound reflects the finding from Fig. 4 that the width of the strip fringing the straight edge over which the cottrellian current is augmented is approximately $3\sqrt{Dt}$. In practice, our integration uses the entire conductor surface $0 \le \chi \le (N-1)\Delta$ of the model, stopping only when the numerical values of the concentration prove to be insignificantly different from the cottrellian concentrations.

The integration in (70) is performed by breaking the integration range into a collection of segments, each of width 2Δ, except for the first, which is 3Δ wide:

$$\frac{\hat{I}(t)}{Fc^{\text{b}}D\ell} = \int_{0}^{N\Delta} \hat{\imath}(\chi,\tau)[1 - \kappa\ell\Delta]\mathrm{d}\chi$$

$$= \int_{0}^{3\Delta} \hat{\imath}(\chi,\tau)[1 - \kappa\ell\Delta]\mathrm{d}\chi + \sum_{n=3,5,\cdots}^{N-3} \int_{n\Delta}^{n\Delta+2\Delta} \hat{\imath}(\chi,\tau)[1 - \kappa\ell\Delta]\mathrm{d}\chi \qquad (71)$$

Because, as Fig. 4 shows, the excess current density changes so dramatically with distance from the edge, we must interpolate carefully between the simulated values, and extrapolate shrewdly into the space between the edge and the $n=1$ point, prior to performing the integration. A vehicle for the interpolation is provided by Eq. (26), which shows, at least for the straight-edge case, that the expression for the current density as a function of x has a leading term in $x^{-1/2}$. Moreover, the cottrellian subtractive contribution to $\hat{\imath}$ is, of course, x-independent. So we base our fitting on the formula

$$\hat{\imath}(\chi,\tau) = (constant) + \left(\begin{array}{c} another \\ constant \end{array}\right)\sqrt{\frac{\Delta}{\chi}} \qquad (72)$$

and fit a relation of this form between consecutive positive odd n values. Each relation is designed to adopt the simulated values $\hat{\imath}_{n,k}$ and $\hat{\imath}_{n+2,k}$ at either end of the segment. This is achieved by the formula

$$\hat{\imath}(\chi,\tau) = \frac{\sqrt{n+2}\,\hat{\imath}_{n+2,k} - \sqrt{n}\,\hat{\imath}_{n,k} + \sqrt{n^2+2n}[\hat{\imath}_{n,k} - \hat{\imath}_{n+2,k}]\sqrt{\Delta/\chi}}{\sqrt{n+2} - \sqrt{n}} \qquad (73)$$

After multiplication by the $1-\kappa\ell\chi$ factor, definite integration now gives

$$\int_{n\Delta}^{n\Delta+2\Delta} \hat{\imath}(\chi,t)[1 - \kappa\ell\chi]\mathrm{d}\chi$$

$$= 2\Delta\left[\begin{array}{l} \frac{\sqrt{n+2}\,\hat{\imath}_{n+2,k} - \sqrt{n}\,\hat{\imath}_{n,k}}{\sqrt{n+2} - \sqrt{n}}[1 - (n+1)\kappa\ell\Delta] + \\ \sqrt{n^2+2n}[\hat{\imath}_{n,k} - \hat{\imath}_{n+2,k}]\left[1 - (2n+2+\sqrt{n^2+2n})\frac{\kappa\ell\Delta}{3}\right] \end{array}\right] \qquad (74)$$

This integral may be written concisely as

$$\int_{n\Delta}^{n\Delta+2\Delta} \hat{\imath}(\chi,t)[1 + \kappa\ell\chi]\,\mathrm{d}\chi = 2\Delta\left[R_{n+2}\hat{\imath}_{n+2,k} + S_n\hat{\imath}_{n,k}\right] \qquad (75)$$

where the R and S quantities may be gleaned from the right-hand side of formula (74). A careful regrouping of a collection of these integrals produces

$$\sum_{n=3,5,\cdots}^{N-1} \int_{n\Delta}^{n\Delta+2\Delta} \hat{r}(\chi,t)[1-\kappa\ell\chi]\,\mathrm{d}\chi$$

$$= 2\Delta\left[R_{N-1}\hat{r}_{N-1,k} + S_3\hat{r}_{3,k} + \sum_{n=5,7,\cdots}^{N-1}(R_n+S_n)\hat{r}_{n,k}\right]$$

$$(76)$$

The sum R_n+S_n is, in fact, the weighting factor denoted W_n in Eq. (63). The solitary R_{N-1} term leads to (66). The $0<\chi<3\Delta$ integral in (70) contributes far more than any other segment. It has to be treated somewhat differently because, though the integral is finite, the integrand is infinite at its lower bound. Accordingly, the fitting to (71) is provided by the $\hat{r}_{1,k}$ and $\hat{r}_{3,k}$ values, which leads to

$$\int_0^{3\Delta} \hat{r}(\chi,\tau)[1-\kappa\ell\chi]\mathrm{d}\chi$$

$$= \frac{3\Delta}{\sqrt{3}-1}\left[\left\{\sqrt{3}-2-\left(\frac{\sqrt{27}}{2}-2\right)\kappa\ell\Delta\right\}\hat{r}_{3,k} + \left\{1-\frac{\kappa\ell\Delta}{2}\right\}\hat{r}_{1,k}\right]$$

$$(77)$$

The coefficient of $\hat{r}_{1,k}$ in this formula is the source of the W_1 term in Eq. (64), while the coefficient of $\hat{r}_{3,k}$, added to S_3, gives W_3 in (65).

Thus it is that a suitably weighted sum of the dimensionless concentrations provides the following expression for the dimensionless excess current:

$$\frac{\hat{I}(t)}{Fc^{\mathrm{b}}D\ell} \Rightarrow \sum_{n=1,3,\cdots}^{N-1} W_n \frac{27\gamma_{n,1,k}-27\beta_{1,k}-\gamma_{n,3,k}+\beta_{3,k}}{12}$$

$$(78)$$

This model is valid for all three cases. For the straight-edge case, the value predicted in Eq. (37) for this dimensionless excess current is 1/2. Using expression (78), the simulation produces values somewhat larger than this, but as the time counter k increases, the values reassuringly approach 0.50. There is no direct interest in simulating currents at the straight edge, however, because the exact theory earlier in this article is unequivocal: the current beyond the cottrellian is solely the prompt current, common to all edges:

$$\hat{I}(t,\mathrm{ii}) = \frac{Fc^{\mathrm{b}}D}{2}\ell$$

$$(79)$$

The excess current is proportional to the length of the edge and to the diffusivity, but time independent.

The motivation for our work is primarily to investigate curved edges, for which no theory presently exists. We seek to find the faradaic current generated by concave and convex edges, over and above the contribution from cottrellian and prompt currents. This is not an easy task, for it is a third order effect that we wish to measure. Therefore, a differential approach is again adopted, in the hope that discretization errors will mostly cancel. Instead of evaluating how the excess current at a curved edge changes with time, we measure the *difference* between the currents at curved edges and those at a straight edge. Three simulations were made, Eq. (78) then being used to compute values of the differences $\hat{I}(t,\mathrm{i})-\hat{I}(t,\mathrm{ii})$ and $\hat{I}(t,\mathrm{iii})-\hat{I}(t,\mathrm{ii})$ undimensioned, in each case, by division by $Fc^{\mathrm{b}}D\ell$. These values are shown plotted versus $\sqrt{k}\Delta$ in Fig. 7. Plotting versus $\sqrt{k}\Delta$ is equivalent to plotting versus the square root of time.

The figure shows that, initially, there is no voltammetric difference between straight and curved edges: they share identical prompt currents. It also shows that additional current flows from curved edges, compared to straight edges, the extra current being positive for concave edges and negative for convex edges. The differences from the straight edge are approximately equal in magnitude, though opposite in sign, showing that the additional current (called the "augmentative current" in the next section) is proportional to the curvature of the edge. Furthermore, Fig. 7 demonstrates that the augmentative current increases as the square root of time. Arguing from the established properties of concave circular edges, as discussed in the next section, we expected the augmentative slope to equal $(\kappa/4)\sqrt{Dt/\pi}$, and the straight lines in the figure correspond to such a
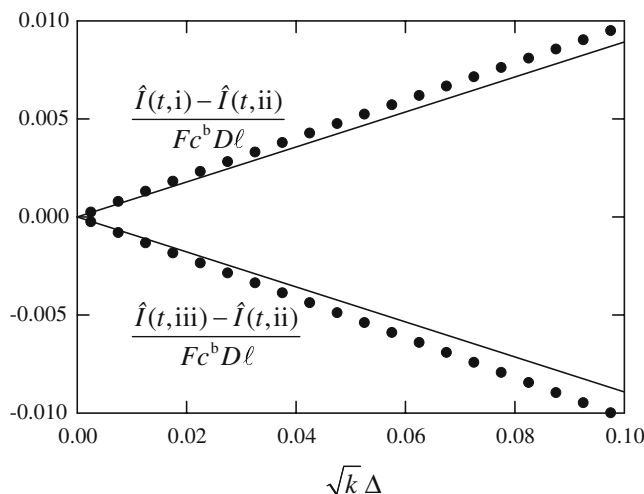

Fig. 7 Graphs of the concavely curved-minus-straight-edged and convexly curved-minus-straight-edged currents plotted versus the square root of time, both the ordinate and the abscissa being suitably normalized. The *points* are derived from simulation, the *straight lines* represent expectations

Fig. 8 Models of partially blocked electrodes. In all four diagrams, *hatching* represents conducting regions of the surface, insulating regions being *shaded grey*. (**a**) represents an "island" of insulator, while (**b**) is a conducting island. The "atoll" topology of (**c**) has an island of insulator within an island of conductor, which is itself within a "sea" of insulator. The geometry of the island in (**d**) results in three places at which proximity effects will diminish the edge current
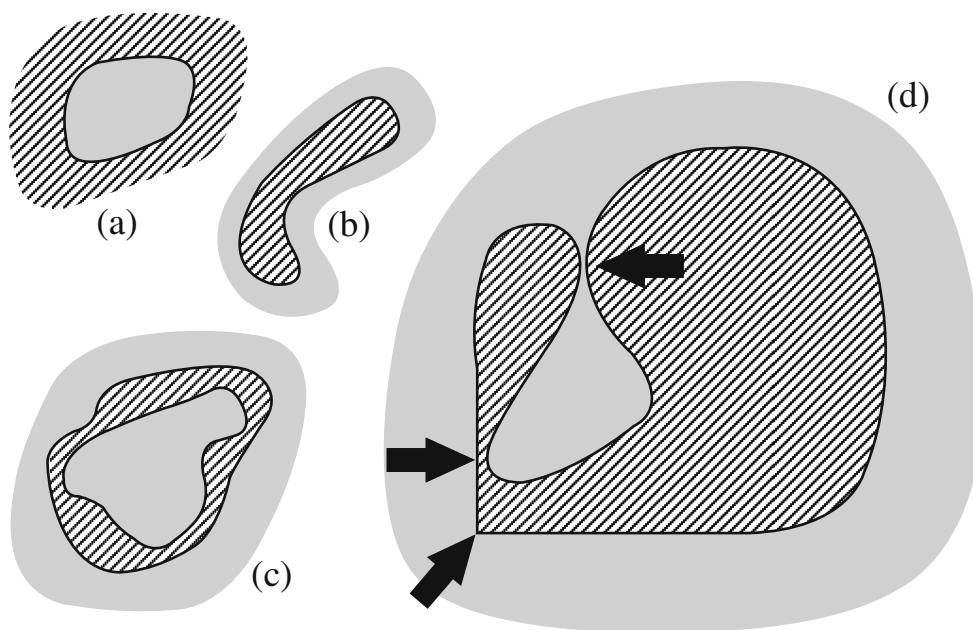
value. Though we could have wished for better, we consider that the agreement between the lines and the points is adequate to confirm our expectation.

Conclusions and applications

We conclude that the response of an edge fragment to a potential jump is the sum of two terms, each proportional to the length of the curve, the second term also being proportional to the curvature of the edge and to the square root of time:

$$\frac{\hat{I}(t)}{Fc^{b}D} = \frac{\ell}{2} + \frac{\kappa\ell}{4}\sqrt{\frac{Dt}{\pi}} \qquad (80)$$

The second right-hand term is positive for concave edges, negative for convex edges, and absent for straight edges. We use the names "prompt" and "augmentative" to distinguish the currents, the latter name reflecting the property of increasing with time, in contrast to the constancy of the prompt current and the evanescent nature of the cottrellian current.

In the context of partially blocked electrodes, edges will rarely have uniform curvature, but they will generally be "closed". That is to say edges will enclose "islands" of either insulator or conductor, as portrayed by (a) and (b) in Fig. 8. The integral of the curvature around a closed curve is the overall angle turned, that is 2π, and therefore the excess current arising from an island is given by

$$\frac{\hat{I}_{\text{island}}(t)}{Fc^{b}D} = \frac{\ell}{2} + \frac{\sqrt{\pi Dt}}{2}\oint \kappa \, \mathrm{d}\ell = \frac{\ell}{2} \pm \sqrt{\pi^{3}Dt} \qquad (81)$$

where the "+" sign in the augmentative term applies to an island of conductor in a "sea" of insulator, and the "−" sign to an island of insulator in a sea of conductor. Interestingly, an "atoll" geometry, as in Fig. 8c, contributes nothing to the augmentative current.

We view Eqs. (80) and (81) as *temporary* descriptors of the chronoamperometric behavior of edges. They become increasingly suspect as time increases. They were derived for isolated edge fragments and ignore any influence that one fragment may have on another. We call any such influence a "proximity effect"; item (d) in Fig. 8 illustrates three circumstances in which this
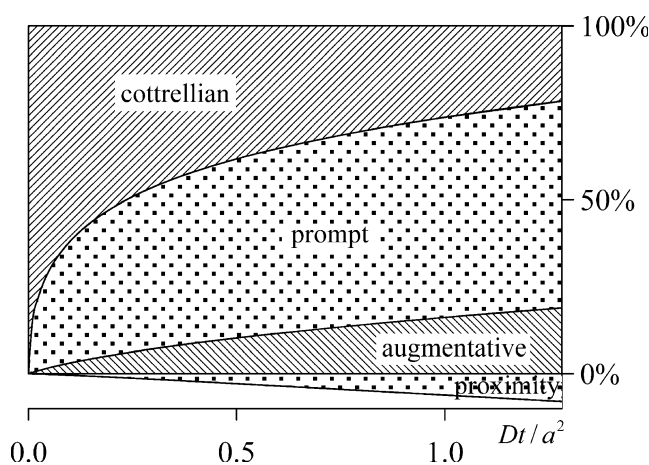
Fig. 9 A diagram showing the contribution of various currents to the total chronoamperometric current at an inlaid disk electrode, as time unfolds. The cottrellian current arises from the surface of the electrode, whereas the prompt current is from its perimeter. The augmentative current has its origin in the curvature of the electrode edge. The "proximity current", which is negative, arises from competition for diffusant between different regions of the edge

effect would be especially severe, limiting the upper time limit for the validity of Eqs. (80) and (81). Proximity always *decreases* the current because two edges are then competing for the diffusing species, so that each goes hungry to some extent. Though it is a crude estimate, proximity effects come into play when the two interfering edges are at a distance of less than about $3\sqrt{Dt}$ from each other.

The only curved edge that has been studied deeply by electrochemists is that separating the conductor and the insulator surfaces in the popular inlaid disk electrode. If such an electrode has a radius a, the conductor has an area α of πa^2; the edge has a length ℓ of $2\pi a$ and a curvature κ of $1/a$. There is no single exact theoretical equation known to describe the one-electron diffusion-controlled current at this electrode, but the five-term expansion

$$\frac{I_{\text{disk}}(t)}{Fc^b D} = a^2 \sqrt{\frac{\pi}{Dt}} + \pi a + \frac{\sqrt{\pi Dt}}{2} - \frac{3\pi Dt}{25a} + \frac{3\pi\sqrt{D^3 t^3}}{226a^2} \quad (82)$$

is known [16] to be valid to parts-per-million accuracy for times up to $t=1.281a^2/D$. When rewritten as

$$\frac{I_{\text{disk}}(t)}{Fc^b D} = \frac{\alpha}{\sqrt{\pi Dt}} + \frac{\ell}{2} + \frac{\kappa \ell}{4}\sqrt{\frac{Dt}{\pi}} - \frac{3\pi Dt}{25a} + \frac{3\pi\sqrt{D^3 t^3}}{226a^2} \quad (83)$$

the first three right-hand terms can be immediately identified as the cottrellian, prompt, and augmentative currents, respectively, while the last two can be assigned to the proximity effect. It is instructive to assess the relative importance of the various currents for the inlaid disk electrode; this is accomplished in Fig. 9. Note that the prompt current is dominant for most of the time, emphasizing the importance of the edge in the voltammetry of this electrode. Beyond the confines of the graph, the prompt current retains its dominance and eventually contributes 79% of the steady-state current.

Other authors [2, 3] have idealized the geometry of partially blocked electrodes by likening them to structures with uniformly sized, neatly arranged shapes on the surface of an otherwise naked electrode. But, without making any preassumption whatsoever about the geometry of a partially blocked electrode, what can be learned from analyzing its response to a potential jump?

Let us suppose that the capacitive current has been carefully eliminated (it, too, can throw light on the geometry of a partially blocked electrode, but that is another story) and that the remaining faradaic response has been analyzed to find the magnitudes of the components with $t^{-1/2}$, t^0, and $t^{1/2}$ time dependences:

$$I(t) = \frac{p}{\sqrt{t}} + q + s\sqrt{t} + \cdots \quad (84)$$

Clearly, the component with $t^{-1/2}$ dependence may be used to find the total area occupied by conductor, because

comparison with the prediction of Cottrell's equation shows that

$$total\ conductor\ area = \sqrt{\frac{\pi}{D}}\frac{p}{Fc^b} \quad (85)$$

The total length of the interfacial lines separating insulator from conductor is directly accessible from the prompt current. One has

$$total\ edge\ length = \frac{2q}{Fc^b D} \quad (86)$$

If the ratio of total conductor area to the overall electrode area A is small, then it is reasonable to assume that the conductor forms islands in a sea of insulator, and that therefore s will be positive. On the other hand, if the conductor area is close to A, then the islands will likely contain insulator and s will be negative. In either event, one can calculate the number of islands from the magnitude of the augmentative current component by the formula

$$number\ of\ islands = \frac{|s|}{Fc^b\sqrt{\pi^3 D^3}} \quad (87)$$

and thence find the average area and perimeter of the islands. For cases in which it is the conductor that constitutes the islands, the formulas are

$$average\ island\ area = \frac{total\ conductor\ area}{number\ of\ islands}$$
$$= \frac{\pi^2 pD}{s} \quad (88)$$

and

$$average\ island\ perimeter = \frac{total\ edge\ length}{number\ of\ islands}$$
$$= \frac{2q\sqrt{\pi^3 D}}{s} \quad (89)$$

Similar relationships apply when the islands are composed of insulator. If both kinds of island exist, it is the difference between the numbers that is significant.

Though relationships (85)–(89) are correct in principle, experimental conditions will need to be favorable to allow their successful exploitation. Being of third order, parameter s will be particularly difficult to measure. One feature of the partially blocked geometry that may be assessed without knowledge of s is the ratio of the area of an average island to its perimeter:

$$average\ (area/perimeter)\ ratio = \frac{p\sqrt{\pi^3 D}}{2q} \quad (90)$$

This is a quantity with the unit of length and could be considered to measure the "grain size" of the conductor/

insulator mosaic. It will be large when the blocking is due to structures of large size, small when it is some microstructure that is responsible.

References

1. Lee C-Y, Guo S-X, Bond AM, Oldham KB (2008) J Electroanal Chem 615:1
2. Amatore C, Saveant J-M, Tessier D (1983) J Electroanal Chem 147:39
3. Davies TJ, Banks CD, Compton RG (2005) J Solid State Electrochem 9:797
4. Arrigan DWM (2004) Analyst 129:1157
5. Fletcher S, Horne MD (1999) Electrochem Commun 1:502
6. Oldham KB (1981) J Electroanal Chem 198:1
7. Boas ML (1973) Mathematical methods in the physical sciences. Wiley, New York
8. Mathews J, Walker RL (1964) Mathematical methods of physics. Benjamin, New York
9. Morse PM, Feshbach H (1953) Methods of theoretical physics. McGraw Hill, Boston
10. Abramowitz M, Stegun AI (1964 and subsequent eds) Handbook of Mathematical Functions, National Bureau of Standards, Washington D.C., chap 13
11. Oldham KB, Myland JC, Spanier J (2008) An atlas of functions second edition. Springer, New York
12. Cottrell FG (1903) Z Phys Chem 42:385
13. Oldham KB (1991) J Electroanal Chem 297:317
14. Britz D (2005) Digital simulation in electrochemistry. Springer, Heidelberg
15. Myland JC, Oldham KB (2005) J Electroanal Chem 576:163
16. Mahon PJ, Oldham KB (2005) Anal Chem 77:6100
17. Gavaghan DJ, Rollett JS (1990) J Electroanal Chem 295:1